NJC

Cite this: *New J. Chem.*, 2012, **36**, 1312–1319

www.rsc.org/njc

**PAPER**

# The catalytic activity of titania nanostructures in the synthesis of amides under solvent-free conditions†

**Sangaraiah Nagarajan,[a] Park Ran,[b] Poovan Shanmugavelan,[a] Murugan Sathishkumar,[a] Alagusundaram Ponnuswamy,*[a] Kee Suk Nahm*[b] and G. Gnana kumar*[c]**

***Received (in Montpellier, France) 17th February 2012, Accepted 29th March 2012***
**DOI: 10.1039/c2nj40119c**



Different shapes and phases of titania nanostructures with the uniform size distribution were synthesized by hydrothermal sol–gel technique. The influence of annealing temperature on the crystalline character, size and phase of the prepared nanomaterials were evidenced from the diffraction analysis. Infrared spectroscopic analysis ensured the structural confirmation of the sulfated titania nanostructures. Catalytic activity of the synthesized nanometric materials in direct amidation of aromatic and aliphatic carboxylic acids with aromatic amines was evaluated. Among the materials studied, sulfated titania nanotubes with the anatase phase exhibited excellent catalytic activity. The employed solvent-free protocol is greener and eradicates the drawbacks associated with the hazardous solvents employed in the prevailing solution phase methodologies.

## 1. Introduction

The booming demand for introducing amide functionality in compounds from pharmaceutical, chemical and natural product sectors[1] has grabbed intensive attention from all corners of the world, in which the connotation of amide formation *via* the coupling of carboxylic acids and amines is highly imperative. As a consequence, newer protocols for amide bond formation have emerged. The most frequently and extensively employed prevailing methodologies involve the direct coupling of amines with carboxylic acids and coupling reagents[2,3] or the coupling of Staudinger's phosphazenes,[4] generated from phosphines and organic azides, with carboxylic acids[5] or its derivatives[6] afford carboxamide. The limitations of these methodologies are the use of benzene (carcinogenic) as the solvent of choice, long reaction times[5a,b] and solubility problems which arise with polar starting substrates.

On the other hand, micro-wave assistance in the coupling of carboxylic acids with amines[7] involves extremely high temperatures. Hence, it has been planned to simplify the preparation procedures of amides, which would avoid the coupling reagents and toxic solvents *via* the utility of an efficient catalyst.

Recently, nanoparticles have emerged as sustainable alternatives to conventional materials in organic reactions, as robust and high surface area catalyst supports due to the large number of active sites per unit area, non-hazardous nature, selectivity, requirement in catalytic amounts, easier reaction work-up, *etc*. The recyclability and easier separation of the solid catalysts improve their competence further.

Despite the aforementioned advantages of nanoparticles, their usage as a catalyst in amide bond formation is relatively new. Among the nanomaterials used, titania nanoparticles have been proven to be excellent catalysts[8] for organic reactions due to their high catalytic activity, selectivity, elevated surface area, easier separation and recyclability. Though titania has been used explicitly as a catalyst for organic reactions, a detailed study on the impact of textural, size and shape of titania nanomaterials over the organic reactions has yet to be understood.

Hence, here in we report the efficiency of the sulfated titania nanoparticles and nanotubes assisted direct coupling of some aromatic amines with various aromatic and aliphatic carboxylic acids under a solvent-free approach to yield the product in just 30 min, which is noteworthy as compared to the titania nanoparticles with long reaction times (3–12 h).[5a,b]

## 2. Results and discussion

The texture, shape, size and phase of the titania nanostructured materials were effectively tuned by a simple hydrothermal sol–gel technique. They were characterized by transmission electron microscopy (TEM), XRD, FTIR, TGA, surface analyzer and catalytic activity of the prepared nanostructured materials in direct amidation is discussed *vide infra*.

[a] *Department of Organic Chemistry, School of Chemistry, Madurai Kamaraj University, Tamilnadu 625 021, India. E-mail: ramradkrish@yahoo.co.in; Tel: +91 9600868323*
[b] *Specialized Graduate School of Hydrogen and Fuel Cell Engineering, Chonbuk National University, Jeonju 561-756, Republic of Korea. E-mail: nahmks@chonbuk.ac.kr; Fax: +82 63 270 2306*
[c] *Department of Physical Chemistry, School of Chemistry, Madurai Kamaraj University, Tamilnadu 625021, India. E-mail: kumarg2006@gmail.com; Tel: +91 9585752997*
† Electronic supplementary information (ESI) available. See DOI: 10.1039/c2nj40119c

 

### 2.1. Morphological images

Fig. 1 exhibits morphological TEM images of the synthesized titania nanoparticles. Fig. 1a clearly reveals the homogeneously distributed titania nanoparticles with diameters of 8–10 nm. The alkoxide precursor was easily hydrolyzed in the water medium and polymerized into a three-dimensional oxide network. Then the three-dimensional network was subjected to the condensation reaction which yielded the titania nanoparticles. Thus, it has been concluded that the titania nanoparticles are produced by the hydrolysis of alkoxide, condensation of the hydrolyzed species, nucleation and growth of primary particles, aggregation of the primary particles and precipitation of large clusters.[9] These reactions can be schematically represented as follows:

$$Ti(OR)_4 + 4H_2O \rightarrow 2Ti(OH)_4 + 4ROH \quad (1)$$

$$Ti(OH)_4 \rightarrow TiO_2\ xH_2O + (2 - x)\ H_2O \quad (2)$$

The as-synthesized 8–10 nm sized nanoparticles were subjected to thermal treatment and an increase in the temperature gradually increased the size of the titania nanoparticles, as shown in Fig. 1b–d. An increase in the temperature increases the aggregation of the prepared nanoparticles which in turn leads to the particle size increase.[10]

The uniform nanotubular structure with a high dispersion in lengths and small diameters were obtained for the synthesized titania nanotubes as shown in Fig. 2a. The tubes were found to be about several hundred nanometers in length and 3–6 nm in diameter. Sodium hydroxide played a major role in the formation of the tubular structure. The synthesized titania particles reacted with sodium hydroxide and lead to a layered alkali titanate. These layered crystals were very thin and were easily exfoliated into individual nanosheets that were highly anisotropic in two-dimensions. Titania sheets were composed of [$TiO_6$] octahedra sharing edges with each other and formed a ribbon structure. Under the high pressure and high temperature, the layered structure rolled up into nanotubes due to the surface tension.[11] During the acid treatment process, $Na^+$ in

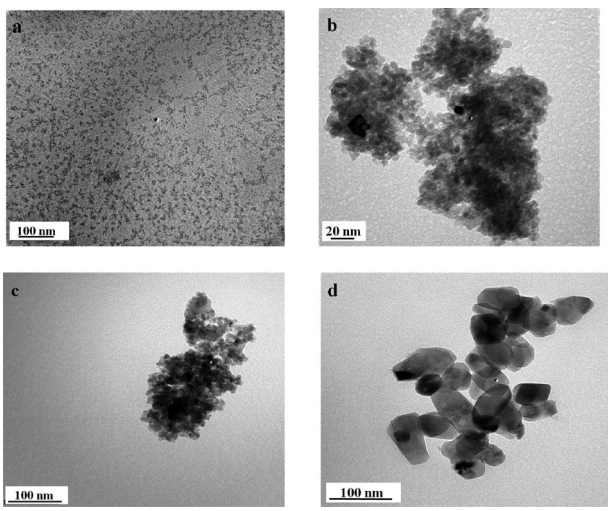


**Fig. 1** Transmission electron microscopic images of the titania nanoparticles (a) before annealing, and after annealing at (b) 400 °C, (c) 600 °C, and (d) 800 °C.

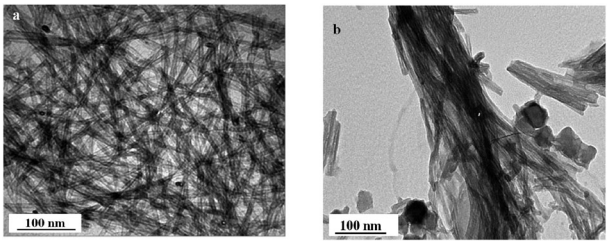


**Fig. 2** TEM images of the titania nanotubes synthesized from (a) as-synthesized (b) 800 °C calcined titania nanoparticles.

the titanate nanotubes is exchanged by $H^+$ which produces the hydrogen titania nanotubes. The hydrate nanotubes are dehydrated by heat treatment, which leads to the formation of pure titania nanotubes. In other words, the nanotubes obtained through the hydrothermal treatment of $TiO_2$ and NaOH, had walls formed by $Ti_3O_7^{2-}$ (titanate) and the interlamellar region would be occupied by $H^+$ ions. Though the diameter of the two kinds of nanotubes is of 3–6 nm, the titania nanotubes prepared from 800 °C calcined titania nanoparticles exhibited a bundle like structure, as shown in Fig. 2b. It may be due to the larger size of its host titania nanoparticles.

### 2.2. X-Ray diffraction studies

Fig. 3 exhibits the diffraction patterns of the synthesized titania particles. The crystalline character of the prepared nanoparticles gets increased with an increase in the temperature. The as-synthesized titania nanoparticles exhibited an anatase phase and were calcined at different temperatures for the phase transformation. Lower temperatures, *i.e.*, 400 °C, does not provide feasibility for the phase transformation (Fig. 3b). The particles annealed at the intermediate temperature, *i.e.*, 600 °C, exhibited rutile and anatase phases (Fig. 3c). The high intensity peaks found at $2\theta = 25.3°$ and 27.30° for the 600 °C calcined titania particles (Fig. 3c) correspond to the (101) and (110) planes of the anatase and rutile phases, respectively.[12,13] It suggests that phase transition from the anatase to the rutile phase gets started at this temperature and the residual anatase phase still exists up to the temperature of 600 °C. But at a higher temperature (800 °C), the anatase residuals were completely removed from the prepared materials, *i.e.*, anatase phase was completely transformed into the rutile phase (Fig. 3d).

Two possible mechanisms, such as the spatial disturbance of the oxygen ion framework and the shifting of the majority of

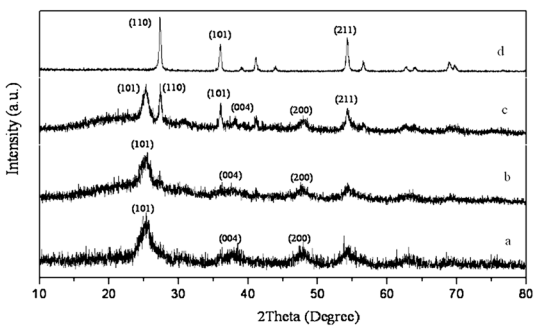


**Fig. 3** XRD patterns of the (a) as-synthesized, and annealed at (b) 400 (C) 600 and (d) 800 °C titania nanoparticles.

the $Ti^{4+}$ ions by breaking two of the six Ti–O bonds to form new bonds were involved in the transformation of the anatase to the rutile phase.[14] Increments in the temperature increased the aggregation or induced contact between the anatase particles and transformed the anatase grains into a large rutile grain. The nucleation and growth can also occur in the bulk or on the surface of a large anatase grain. The growth of the rutile grain may happen when a rutile crystallite comes into contact with an anatase crystallite forming a larger rutile crystallite or when two rutile nuclei merge together. The nucleation and growth of the prepared titania nanoparticles effectively occurred at 800 °C. It also suggests that after the nucleation processes the growth process started immediately. Since the titania nanotubes were produced from the titania particles, the phase of the titania nanotubes purely depend on their host titania nanoparticles (Fig. 4a and b) and the phase transformation did not occur for the titania nanotubes. There were no morphological and diffraction changes observed between the bare and sulfated titania nanoparticles and nanotubes.

### 2.3. Structural characterization

Structural confirmation of the sulfated titania nanotubes was characterized by infrared spectroscopy (see ESI†) and the obtained peaks are assigned as follows: intensive bands observed at 3437 and 1636 $cm^{-1}$ are attributed to the stretching vibration of hydroxyl groups and adsorbed water molecules, respectively.[15] The S=O stretching of the sulfated titania nanotubes were found at 1052 and 1132 $cm^{-1}$, which represent the successful implantation of sulfonic acid moieties over the titania nanotubes. Significant bands observed in the region of 400–1000 $cm^{-1}$ represent the Ti–O framework stretching frequencies.

### 2.4. Thermal behavior

Fig. 5 depicts the thermogravimetric analysis of bare and sulfated titania nanotubes. The prepared samples exhibited continuous weight losses at lower temperatures and continued at the higher temperatures. The bare titania nanotubes (Fig. 5a) exhibited a significant weight loss at 80–100 °C and this is attributed to the evaporation of physisorbed and interlayer water molecules. The sulfated titania nanotubes (Fig. 5b) exhibited two significant weight losses at 80–100 °C and 300–345 °C and are attributed to the evaporation of physisorbed and interlayer water molecules and the decomposition of sulfonic acid moieties, respectively. The sulfated titania nanotubes exhibited a lower thermal stability than that of bare titania nanotubes due to its high hydrophilic character. Though the prepared nanotubes exhibited continuous weight losses, the lower weight loss observed from the spectrum guaranteed its higher thermal stability.

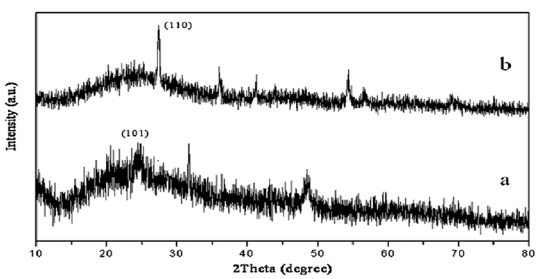


**Fig. 4** XRD pattern of titania nanotubes prepared from the (a) synthesized titania nanoparticles, and the (b) 800 °C calcined titania nanoparticles.

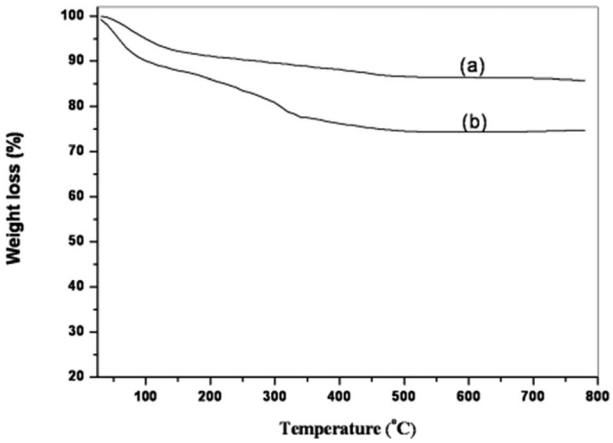


**Fig. 5** Thermogravimetric analysis of (a) bare and (b) sulfated titania nanotubes.

### 2.5. Textural properties

The specific surface area of the prepared titania nanoparticles are given in Table 2. The as-synthesized nanoparticles exhibited higher surface areas than those of the calcined samples due to their smaller crystallite size.[16] But an increase in the temperature effectively increased the crystallite size of the prepared materials which decreases the surface area of the corresponding materials. As shown in Table 2, the surface area decreased for the calcined samples. The conversion of titania nanoparticles into titania nanotubes effectively increases the surface area and is purely attributed to the tubular shape of the prepared sample. The sulfonation process effectively increased the surface area of the corresponding nanomaterials and its influence on catalytic activity will be discussed later.

### 2.6. Catalytic activity of the titania nanostructured materials on amide synthesis

The aim of the present work is to investigate and characterize the activity of nanometric titania particles as the heterogeneous catalyst for direct amidation. To investigate the catalytic activity of the titania nanoparticles, phenyl acetic acid **1a** has been chosen as a representative substrate and was reacted with aniline at 110 °C for 30 min under solvent-free conditions.

In the absence of a catalyst (Table 1, entry 1), amide was formed in 45% yield. The catalyst amount was varied over a range of 0–30 wt% of total mass of the reactants. Increasing the catalyst concentration increases the number of active sites. The increased number of active sites promote the number of contact sites between the catalyst and substrates, and this gets reflected in the yield of the amide formation. Table 1 indicates that the yield of the amide formation is directly proportional to the amount of catalyst used and reaches a constant at about 24 wt%. It has been assumed that the active sites which has been provided by the catalyst up to 24 wt% has been effectively used by the substrates and beyond which the active sites are not used up by the organic substrates. From the obtained values,

 

**Table 1** Screening of wt% of the catalyst in the synthesis of *N*,2-diphenylacetamide

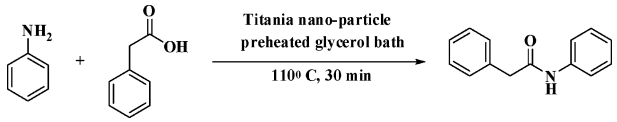


| Entry | Concentration of catalyst (wt%) | Yield[a] (%) |
|---|---|---|
| 1 | 0 | 45 |
| 2 | 10 | 61 |
| 3 | 15 | 67 |
| 4 | 20 | 71 |
| 5 | 22 | 74 |
| 6 | 24 | 77[b] |
| 7 | 26 | 77 |
| 8 | 30 | 77 |

[a] Isolated yield. [b] Optimized wt% of catalyst.

24 wt% has been chosen as minimum concentration of the catalyst for effectual amide formation and has been used for further studies.

In the study, direct amidation was investigated with and without catalyst at 110 °C, the reaction time being 30 min. Also interestingly the nature of the catalyst employed had an impact on the yield of the product. Replacing the as-synthesized nanoparticles with the 800 °C calcined nanoparticles (Table 2, entry 3) had no promising improvement as it afforded only 71% of the amide. This observation is purely attributed to the calcined particles having lower surface areas, as influenced by their larger particle sizes. The other calcined (400 & 600 °C) particles also exhibited lower catalytic activities due to their larger particle sizes (data not shown). However, the titania nanotubes increased the yield of amide formation due to its high surface area achieved *via* its tubular structure. The surface area of the catalyst played a vital role in determining the yield of amide formation. The increased surface area provides a higher number of active sites and induces higher contact between the catalyst and substrates. In addition, the sulfonation (sulfur content) of catalysts also plays a role in determining the yield of a reaction (Table 2). The sulfur content of the studied titania nanostructures has been measured by EDX analysis (Table 2). The sulfur content of the calcined titania nanoparticles is decreased as compared to the as-synthesized titania nanoparticles, which is due to their larger size and lower surface area. A higher sulfur content was obtained for the titania nanotubes prepared from the as-synthesized titania nanoparticles than for the as-synthesized titania nanoparticles, and this is purely attributed to their high surface area. Since the surface to volume ratio is higher for the nanotubes as compared to the nanoparticles, the nanotubes adsorbed higher amounts of sulfonic acid moieties. Hence, the sulfated titania nanotubes exhibited a higher sulfur content and this gets reflected in the yield of amide formation, the best affording 98% yield. The titania nanotubes prepared from the as-synthesized titania nanoparticles exhibited a higher number of hydroxyl groups over their surfaces and exhibited a high hydrophilic character. However, the titania nanotubes prepared from the calcined titania nanoparticles lost the hydroxyl groups from their surfaces due to the calcination process, which yielded a lower hydrophilic nature. Effective sulfonation could be achieved only when the proper hydrophilic compatibility was maintained between the heat matrix and the sulfuric acid. This was more effectively satisfied by the titania nanotubes prepared from the as-synthesized titania nanoparticles than by the titania nanotubes prepared from the calcined titania nanoparticles due to the higher number of hydroxyl groups.

The above screening revealed that both the sulfated titania nanoparticles (Table 2, entry 5) and the nanotubes (Table 2, entry 6) exhibited very good catalytic activity compared to the conventional reaction (absence of a catalyst) (Table 1, entry 1). In particular, the sulfated titania nanotubes with the highest surface area was found to be the best catalyst, affording 98% of the amide in just 30 min (Table 2, entry 5). In the present study, the rate of amidation is enhanced prominently by using sulfated titania nanotubes compared to a recent report on amidation catalyzed by titania nanoparticles[8] wherein the reaction time has been reported to be 3 h.

Subsequently, the reusability of the sulfated titania nanotubes was established and summarized in Table 3. The sulfated titania nanotubes allowed for a robust recycling capability, with well-retained activity of 80% even after the sixth cycle under the same reaction conditions. An increase in the number

**Table 2** Effect of titania nanocatalysts for the formation of *N*,2-diphenylacetamide

| Entry | Catalyst | Phase | Surface area ($m^2\ g^{-1}$) | EDX Elemental analysis(%) | | | Yield[a] (%) |
|---|---|---|---|---|---|---|---|
| | | | | Ti | O | S | |
| 1 | As-synthesized titania nanoparticles | Anatase | 229 | 35.44 | 64.56 | — | 77 |
| 2 | Nanotubes produced from as-synthesized titania nanoparticles | Anatase | 298 | 35.38 | 64.62 | — | 81 |
| 3 | Titania nanoparticles calcined at 800 °C | Rutile | 22 | 35.80 | 64.20 | — | 71 |
| 4 | Titania nanotubes prepared from 800 °C calcined titania nanoparticles | Rutile | 56.7 | 35.88 | 64.12 | — | 74 |
| 5 | Sulfated titania nanoparticles | Anatase | 252 | 34.64 | 64.11 | 1.25 | 83 |
| 6 | Sulfated titania nanotubes | Anatase | 319 | 34.34 | 63.7 | 1.96 | 98 |
| 7 | Sulfated titania nanoparticles prepared from 800 °C calcined titania nanoparticles | Rutile | 38 | 34.88 | 64.23 | 0.89 | 75 |
| 8 | Sulfated titania nanotubes prepared from 800 °C calcined titania nanoparticles | Rutile | 43.6 | 34.74 | 64.17 | 1.09 | 79 |

Reaction conditions: phenylacetic acid (200 mg, 1.4 mmol), aniline (136 mg, 1.4 mmol) and catalyst (24 wt%) for 30 min in preheated glycerol bath (110 °C–120 °C).[a] Isolated yield.

**Table 3** Catalyst reusability and sulfur content in amide synthesis

| Entry | Recycle no. | % Yield of *N*,2-diphenylacetamide | Sulfur content (%) |
|---|---|---|---|
| 1 | Fresh | 98 | 1.96 |
| 2 | First recycle | 94 | 1.82 |
| 3 | Second recycle | 90 | 1.67 |
| 4 | Third recycle | 87 | 1.53 |
| 5 | Fourth recycle | 85 | 1.38 |
| 6 | Fifth recycle | 83 | 1.25 |
| 7 | Sixth recycle | 80 | 1.12 |

of cycles detaches the sulfonic acid moieties, *i.e.*, loss of sulfonic acid moieties from the titania nanotubes, as revealed from the EDX analysis (Table 3). A gradual decrease in the sulfur content decreases the catalytic activity of the sulfated titania nanotubes. In addition, a slight increase in the particle size and porosity coverage of the titania nanostructures over the repetitive cycles decreases the surface area, which reflects in the gradual decrement of the amide formation yield.

In continuation of the above preliminary optimization, the broad scope of the sulfated nanotubes as catalyst was established by synthesizing structurally diversified amides which are depicted in Table 4. The products were interpreted by $^{1}H$ and $^{13}C$ NMR (ESI†).

## 3. Conclusion

The impact of the texture, shape, size and phase of the titania nano-materials in catalyzing the direct amidation of aromatic and aliphatic carboxylic acids with some aromatic amines under solvent-free conditions has been examined. Although all of them exhibited good catalytic activities compared to the catalyst-free conditions, the sulfated titania nanotubes were found to be the best catalyst and hence they were used to synthesize a variety of amides. The catalytic activity was very promising and affords the amides in good to excellent yields in short reaction times at relatively lower temperature. Thus, the study conveys the fact that the sulfated titania nanotubes are an efficient catalyst as compared to other corresponding nanosized materials in amide synthesis *via* a solvent-free green protocol eradicating the limitations associated with the hazardous solvents used in the prevailing solution phase protocols.

## 4. Experimental

### 4.1. Characterizations

All chemicals and solvents were of commercially high purity grade purchased from Acros Organics Synthesis Pvt. Ltd. and Sigma-Aldrich Ltd, India. Melting points (mp) were obtained on electro-thermal apparatus and are uncorrected. Conventional transmission electron micrographs were recorded on a JEOL JEM-2010 transmission electron microscope equipped with an energy-dispersive X-ray spectroscopy (EDX). X-Ray diffraction patterns of the prepared materials were characterized using a (D-Max-3A, Rigaku XRD) diffractometer. FT-IR spectra of the sulfated titania nanotubes was recorded between 400–4000 $cm^{-1}$ transmittance mode using a Jasco FT-IR spectrophotometer. Textural properties of the prepared materials

**Table 4** Sulfated titania nanotubes catalyzed amide syntheses at 110 °C

| Entry | Amine | Acid | Amide | Yield (%) |
|---|---|---|---|---|
| 1 |  |  | 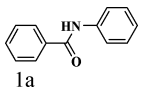 1a | 75 |
| 2 |  | 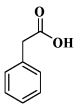 | 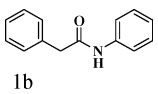 1b | 98 |
| 3 |  | 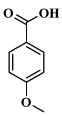 | 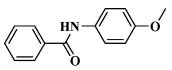 1c | 75 |
| 4 |  | 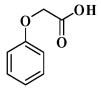 | 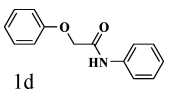 1d | 93 |
| 5 |  |  | 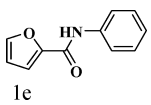 1e | 85 |
| 6 |  | 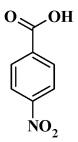 | 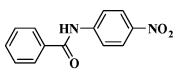 1f | 77 |
| 7 |  | 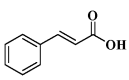 | 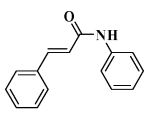 1g | 87 |
| 8 |  | 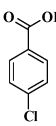 | 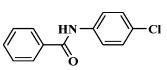 1h | 81 |
| 9 |  |  | 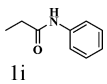 1i | 92 |
| 10 |  | 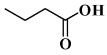 | 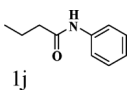 1j | 94 |
| 11 |  | 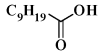 | 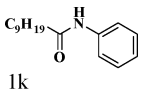 1k | 95 |
| 12 | 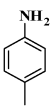 | 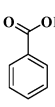 | 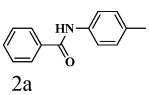 2a | 75 |

 

**Table 4** (*continued*)

| Entry | Amine | Acid | Amide | Yield (%) |
|---|---|---|---|---|
| 13 |  | 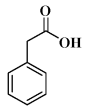 | 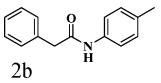 2b | 91 |
| 14 | 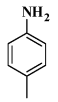 |  | 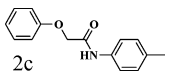 2c | 86 |
| 15 |  |  | 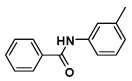 3a | 79 |
| 16 |  |  | 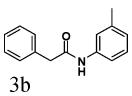 3b | 92 |
| 17 |  |  | 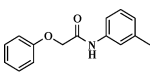 3c | 90 |

were characterized using a BET surface area analyzer BELSORP. Thermal behavior of the prepared nanostructured materials was examined on a Perkin-Elmer (Wellesley, MA) instrument under a nitrogen atmosphere at a heating rate of 20 °C $min^{-1}$ from 30 to 800 °C. $^1$H NMR and $^{13}$C NMR spectra were recorded in $CDCl_3$ on a Bruker Avance 300 MHz spectrometer and the chemical shifts are reported as $\delta$ values in parts per million (ppm) relative to tetramethylsilane, with $J$ values in Hertz. The splitting patterns in the $^1$H NMR spectra are reported as follows: s = singlet; d = doublet; t = triplet; q = quartet; m = multiplet. $^{13}$C NMR data are reported with the solvent peak ($CDCl_3$ = 77.0) as the internal standard. The spectral data of all known compounds are consistent with those reported previously.

### 4.2. Synthesis of titania nanoparticles

Ti(IV)-iso propoxide solution was injected in to the 5 M HCl aqueous solution and magnetically stirred for 1 h. Then the prepared nanoparticles were centrifuged and were annealed at 400, 600 and 800 °C for the phase determination/transformation studies.

### 4.3. Synthesis of titania nanotubes

A stipulated amount of freshly prepared titania nanoparticles was suspended in 20 mL of 10 M sodium hydroxide aqueous solution. The resulting suspension was taken in a teflon vessel and placed in an autoclave at 150 °C for 20 h. Then the samples were washed with 0.1 N HCl aqueous solution, deionized water, and were subsequently separated *via* the centrifugation method. This procedure was repeated until the washing solution reached a pH < 7.

### 4.4. Acidification of titania nanoparticles and nanotubes

For the sulfonation process, the freshly prepared titania nanoparticles and nanotubes were impregnated in 0.5 M of sulfuric acid for 24 h at room temperature. Then the materials were centrifuged and then dried at 100 °C. The samples were washed with deionized water, and were subsequently separated *via* the centrifugation method. This procedure was repeated until the washing solution reached a pH < 7.

### 4.5. Typical procedure for the preparation of amides

A mixture of phenylacetic acid (200 mg, 1.4 mmol), aniline (136 mg, 1.4 mmol) and catalyst (80 mg, 24 wt% (W/W) in a microwave vial (10 mL), and was heated at 110 °C for 30 min in a preheated glycerol bath. Then the mixture was diluted with ethylacetate (10 mL) and centrifuged to remove the catalyst. The filtrate was washed with 10% $NaHCO_3$ (10 mL) and dried over anhydrous magnesium sulphate. The solvent was then removed under reduced pressure to give the amide (yield: 98%).

### 4.6. Analytical data

***N*-Phenylbenzamide**[17] **1a.** White solid; mp 163–164 °C; yield: 75%; molecular formula:$C_{13}H_{11}NO$; $^1$H NMR (300 MHz, $CDCl_3$) $\delta$ 7.13–7.86 (m, 10H); $^{13}$C NMR (75 MHz, $CDCl_3$) $\delta$ 165.73, 146.30, 137.88, 134.96, 131.82, 129.24, 129.07, 128.76, 126.98, 124.55, 120.17, 118.53, 115.08. Commercial compound

***N*,2-Diphenylacetamide**[18] **1b.** White solid; mp 118–119 °C; yield: 98%; molecular formula: $C_{14}H_{13}NO$; $^1$H NMR (300 MHz, $CDCl_3$) $\delta$ 6.67–7.42 (m, 10H), 3.72 (s, 2H); $^{13}$C NMR (75 MHz, $CDCl_3$) $\delta$ 169.14, 137.60, 134.40, 129.50, 129.52, 129.19, 128.91, 127.63, 124.44, 119.83, 118.52, 115.07, 44.77.

***N*-(4-Methoxyphenyl)benzamide**[19] **1c.** White solid; mp 147–157 °C; yield: 75%; molecular formula: $C_{14}H_{13}NO_2$; $^1$H NMR (300 MHz, $CDCl_3$) $\delta$ 8.22–6.67 (m, 10H), 3.87 (s, 2H); $^{13}$C NMR (75 MHz, $CDCl_3$) $\delta$ 165.19, 138.224, 129.08, 128.90, 124.377, 120.22, 114.08, 55.48.

**2-Phenoxy-*N*-phenylacetamide**[20] **1d.** White solid; mp 99–100 °C; yield: 93%; molecular formula: $C_{14}H_{13}NO_2$; $^1$H NMR (300 MHz, $CDCl_3$) $\delta$ 8.33 (bs, 1H), 7.622–6.98 (m, 10H), 6.60 (s, 2H); $^{13}$C NMR (75 MHz, $CDCl_3$) $\delta$ 166.25, 157.12, 136.93, 129.89, 129.05, 124.83, 122.47, 120.17, 114.93, 67.77.

***N*-Phenylfuran-2-carboxamide**[21] **1e.** White solid; mp 131–132 °C; Yield: 85%; Molecular Formula: $C_{11}H_9NO_2$; $^1$H NMR (300 MHz, $CDCl_3$) $\delta$ 8.08 (bs, 1H), 7.67–6.55 (m, 8H); $^{13}$C NMR (75 MHz, $CDCl_3$) $\delta$ 155.96, 147.89, 144.04, 137.36, 129.03, 124.45, 119.88, 115.13, 112.52.

***N*-(4-Nitrophenyl)benzamide**[8] **1f.** White solid; mp 162–164 °C; yield: 77%; pale yellow solid; mp = 199 °C; molecular formula: $C_{13}H_{10}N_2O_3$; $^1$H NMR (300 MHz, $CDCl_3$) $\delta$ 10.31 (bs, 1H), 8.34–7.125 (m, 10H); $^{13}$C NMR (75 MHz, $CDCl_3$) $\delta$ 163.12, 158.32, 14.03, 137.29, 127.88, 127.30, 123.03, 121.96, 119.66.

***N*-Phenylcinnamamide[22] 1g.** White solid; mp 1501–152 °C; yield: 87%; molecular formula: $C_{15}H_{13}NO$; $^1$H NMR (300 MHz, $CDCl_3$) $\delta$ 8.46 (bs, 1H), 7.75 (d, $J$ = 15.9 Hz, 1H); 7.69–7.09 (m, 10H), 6.71 (d, $J$ = 15.6 Hz, 1H); $^{13}$C NMR (75 MHz, $CDCl_3$) $\delta$ 163.12, 158.32, 14.03, 137.29, 127.88, 127.30, 123.03, 121.96, 119.66.

***N*-(4-Chlorophenyl)benzamide[23] 1h.** White solid; mp 199–200 °C; yield: 81%; molecular formula: $C_{13}H_{10}ClNO$; $^1$H NMR (300 MHz, $CDCl_3$) $\delta$ 8.12–7.16 (m, 10H); $^{13}$C NMR (75 MHz, $CDCl_3$) $\delta$ 164.60, 140.21, 138.13, 137.64, 133.35, 131.52, 129.09, 129.01, 128.81, 128.40, 124.77, 120.28.

***N*-Phenylpropionamide[24] 1i.** White solid; mp 105–106 °C; yield: 92%; molecular formula: $C_9H_{11}NO$; $^1$H NMR (300 MHz, $CDCl_3$) $\delta$ 8.39 (bs, 1H), 7.56–7.05 (m, 5H), 2.37 (q, $J$ = 7.5 Hz, 2H), 1.20 (t, $J$ = 7.5 Hz, 3H); $^{13}$C NMR (75 MHz, $CDCl_3$) $\delta$ 129.18, 128.74, 124.30, 120.18, 115.08.

***N*-Phenylbutyramide[25] 1j.** White solid; mp 82–84 °C; yield: 94%; molecular formula: $C_{10}H_{13}NO$; $^1$H NMR (300 MHz, $CDCl_3$) $\delta$ 8.51 (bs, 1H), 7.57–6.66 (m, 5H), 2.31 (t, $J$ = 7.5 Hz, 2H), 1.71 (sextet, $J$ = 7.5 Hz, 2H), 0.95 (t, $J$ = 7.5 Hz, 3H); $^{13}$C NMR (75 MHz, $CDCl_3$) $\delta$ 172.12, 138.02, 129.02, 123.89, 120.10, 118.28, 114.96, 39.12, 18.93, 13.45.

***N*-Phenyldecanamide[26] 1k.** White solid; mp 66–68 °C; yield: 95%; molecular formula: $C_{16}H_{25}NO$; $^1$H NMR (300 MHz, $CDCl_3$) $\delta$ 7.52–7.06 (m, 5H), 4.4 (bs, 1H), 2.34 (t, $J$ = 7.5 Hz, 2H), 1.74–1.26 (m, 14H), 0.87 (t, $J$ = 6.3 Hz, 3H); $^{13}$C NMR (75 MHz, $CDCl_3$) $\delta$ 172.73, 145.68, 138.14, 129.23, 128.83, 124.19, 120.32, 119.16, 115.81, 37.47, 34.30, 31.91, 29.53, 29.46, 29.31, 29.15, 25.79, 24.88, 22.70, 14.11.

***N*-*p*-Tolylbenzamide[8] 2a.** White solid; mp 155–157 °C; yield: 75%; molecular formula: $C_{14}H_{13}NO$; $^1$H NMR (300 MHz, $CDCl_3$) $\delta$ 7.92–7.10 (m, 10H), 2.33 (s, 3H); $^{13}$C NMR (75 MHz, $CDCl_3$) $\delta$ 165.67, 135.48, 135.21, 134.24, 131.69, 129.59, 128.75, 127.04, 120.41, 20.88.

**2-Phenyl-*N*-*p*-tolylacetamide[27] 2b.** White solid; mp 131–132 °C; yield: 91%; molecular formula: $C_{15}H_{15}NO$; $^1$H NMR (300 MHz, $CDCl_3$) $\delta$ 7.37–7.05 (m, 10H), 3.68 (s, 2H), 2.28 (s, 3H); $^{13}$C NMR (75 MHz, $CDCl_3$) $\delta$ 169.12, 135.13, 134.04, 129.47, 129.36, 129.09, 127.50, 120.03, 44.66, 20.80.

**2-Phenoxy-*N*-*p*-tolylacetamide[28] 2c.** White solid; mp 97–99 °C; yield: 86%; molecular formula: $C_{15}H_{15}NO_2$; $^1$H NMR (300 MHz, $CDCl_3$) $\delta$ 8.2 (bs, 1H), 7.45-6.95 (m, 9H), 2.15 (s, 2H), 2.30 (s, 3H); $^{13}$C NMR (75 MHz, $CDCl_3$) $\delta$ 166.04, 157.08, 134.48, 134.26, 129.49, 122.38, 120.14, 114.48, 67.70, 20.76.

***N*-*m*-Tolylbenzamide[29] 3a.** White solid; mp 117–118 °C; yield: 79%; molecular formula: $C_{14}H_{13}NO$; $^1$H NMR (300 MHz, $CDCl_3$) $\delta$ 7.92 (bs, 1H), 7.85–6.94 (m, 9H), 2.34 (s, 3H); $^{13}$C NMR (75 MHz, $CDCl_3$) $\delta$ 165.67, 138.94, 137.88, 135.13, 131.66, 128.82, 128.68, 126.96, 125.33, 120.92, 117.34, 21.38.

**2-Phenyl-*N*-*m*-tolylacetamide 3b.** White solid; mp 85–87 °C; yield: 92%; molecular formula: $C_{15}H_{15}NO_2$; $^1$H NMR (300 MHz, $CDCl_3$) $\delta$ 7.92 (bs, 1H), 7.85–6.94 (m, 9H), 2.34 (s, 3H); $^{13}$C NMR (75 MHz, $CDCl_3$) $\delta$ 165.67, 138.94, 137.88, 135.13, 131.66, 128.82, 128.68, 126.96, 125.33, 120.92, 117.34, 21.38.

**2-Phenoxy-*N*-*m*-tolylacetamide 3c.** White solid; mp 93–94 °C; yield: 90%; molecular formula: $C_{15}H_{15}NO_2$; $^1$H NMR (300 MHz, $CDCl_3$) $\delta$ 8.25 (bs, 1H), 7.42–6.95 (m, 9H), 4.59 (s, 2H), 2.35 (s, 3H); $^{13}$C NMR (75 MHz, $CDCl_3$) $\delta$ 166.15, 157.02, 138.99, 136.73, 129.85, 128.85, 125.63, 122.40, 120.70, 117.18, 114.83, 67.64, 21.39.

## Acknowledgements

The authors thank IRHPA, DST for providing the 300 MHz NMR instrument for recording the NMR spectra and S. N. and P. S. acknowledge their grateful thanks to UGC for the sanction of UGC(BSR)–JRF meritorious fellowship. P. R. and K. S. were supported by the Human Resources Development of the Korea Institute of Energy Technology Evaluation and Planning (Ketep) grant funded by the Korean government Ministry of Knowledge Economy.

## References

1 (*a*) T. Fredrik and A. Hans, *Org. Biomol. Chem.*, 2010, **8**, 4536; (*b*) N. Zenker, L. S. Hubbard and W. Wright, *J. Nat. Prod.*, 1988, **51**, 862; (*c*) T. S. Jagodzinski, *Chem. Rev.*, 2003, **103**, 197.
2 (*a*) W. Heal, J. Mark Thompson, R. Mutter, H. Cope, J. C. Louth and B. Chen, *J. Med. Chem.*, 2007, **50**, 1347; (*b*) P. J. Dunn, S. Galvin and K. Hettenbach, *Green Chem.*, 2004, **6**, 43; (*c*) M. J. Petersson, C. Marchal, W. A. Loughlin, I. D. Jenlins, P. C. Healy and A. Almesaker, *Tetrahedron*, 2007, **63**, 1395; (*d*) S. T. Kadam and S. S. Kim, *Synthesis*, 2008, **2**, 267.
3 P. T. Anastas and T. C. Williamson, *Green Chemistry: Frontiers in Benign Chemical Synthesis and Processes*, Oxford University Press, Oxford, 1988.
4 (*a*) H. Staudinger and J. Meyer, *Helv. Chim. Acta*, 1919, **2**, 635; (*b*) Y. G. Gololobov, I. N. Zhmurova and L. F. Kasukhin, *Tetrahedron*, 1981, **37**, 437; (*c*) Y. G. Gololobov and L. F. Kasukhin, *Tetrahedron*, 1992, **48**, 1353; (*d*) M. Sathishkumar, P. Shanmuga velan, S. Nagarajan, M. Maheswari, M. Dinesh and A. Ponnuswamy, *Tetrahedron Lett.*, 2011, **52**, 2830.
5 (*a*) J. Garica, F. Urpi and J. Vilarrasa, *Tetrahedron Lett.*, 1984, **25**, 4841; (*b*) L. Kovacs, E. Osz, V. Domokos, W. Holzer and Z. Gyorgydesk, *Tetrahedron*, 2001, **57**, 4609; (*c*) J. P. Malkinson, R. A. Falconer and I. J. Toth, *J. Org. Chem.*, 2000, **65**, 5249; (*d*) F. Urpi and F. J. Vilarrasa, *Tetrahedron Lett.*, 1986, **27**, 4623.
6 (*a*) D. E. Shalev, S. M. Chiacchiera, A. E. Radkowsky and E. M. Kosower, *J. Org. Chem.*, 1996, **61**, 1689; (*b*) I. Bosch, A. Gonzalez, F. Urpi and J. Vilarrasa, *J. Org. Chem.*, 1996, **61**, 5638.
7 E. Gelens, L. Smeets, L. A. J. M. Sliedregt, B. J. van Steen, C. G. Kruse, R. Leursa and R. V. A. Orrua, *Tetrahedron Lett.*, 2005, **46**, 3751.
8 M. Hosseini-Sarvari, E. Sodagar and M. M. Doroodmand, *J. Org. Chem.*, 2011, **76**, 2853.
9 D. Vorkapic and T. Matsoukas, *J. Am. Ceram. Soc.*, 1998, **81**, 2815.
10 Y. Zhao, C. Li, X. Liu, F. Gu, H. Jiang, W. Shao, L. Zhang and Y. He, *Mater. Lett.*, 2007, **61**, 79.
11 D. Wang, F. Zhou, Y. Liu and W. Liu, *Mater. Lett.*, 2008, **62**, 1819.
12 P. W. Murray, N. G. Condon and G. Thornton, *Phys. Rev. B*, 1995, **51**, 10989.
13 S. Rather, N. Mehraj-ud-din, R. Zacharia, S. W. Hwang, A. R. Kim and K. S. Nahm, *Int. J. Hydrogen Energy*, 2009, **34**, 961.
14 O. K. Varghese, D. Gong, M. Paulose, C. A. Grimes and E. C. Dickey, *J. Mater. Res.*, 2003, **18**, 156.
15 Z. Wang, F. Zhang, Y. Yang, B. Xue, J. Cui and N. Guan, *Chem. Mater.*, 2007, **19**, 3286.
16 H. Chen, K. Dai, T. Peng, H. Yang and D. Zhao, *Mater. Chem. Phys.*, 2006, **96**, 176.

 

17 R. H. Lawrence, S. A. Biller, O. M. Fryszman and M. A. Poss, *Synthesis*, 1997, 553.
18 S. Chaudhari, S. D. Salim, R. V. Sawant and K. G. Akamanchi, *Green Chem*., 2010, **12**, 1707.
19 V. P. Srivastava, R. Patel, Garima and L. D. S. Yadav, *Chem. Commun*., 2010, **46**, 5808.
20 C. R. Harrison, P. Hodge, B. J. Hunt, E. Khoshdel and G. Richardson, *J. Org. Chem*., 1983, **48**, 3721.
21 K. N. Kumar, K. Sreeramamurthy, S. Palle, K. Mukkanti and P. Das, *Tetrahedron Lett*., 2005, **51**, 899.
22 S. Ueda, T. Okada and H. Nagasawa, *Chem. Commun*., 2010, **46**, 2462.
23 L. Zhang, S. Su, H. Wu and S. Wang, *Tetrahedron*, 2009, **65**, 10022.
24 J. W. Comerford, J. H. Clark, D. J. Macquarrie and S. W. Breeden, *Chem. Commun*., 2009, 2562.
25 A. R. Katritzky, R. Jiang, G. L. Sommen and S. K. Singh, *ARKIVOC*, 2004, **9**, 44.
26 L. Perreux, A. Loupy and F. Volatron, *Tetrahedron*, 2002, **58**, 2155.
27 Z. Zhang, Y. Yu and L. S. Liebeskind, *Org. Lett*., 2008, **10**, 3005.
28 O. P. Bansal, J. S. Srinivas and C. V. Sastry Reddy, *Indian J. Chem., Sect. B: Org. Chem. Incl. Med. Chem*., 1992, **31**, 289.
29 A. Correa and C. Bolm, *Angew. Chem., Int. Ed*., 2007, **46**, 8862.